Chapter 6
Characterizing the Topography of a Potential Energy Surface

6.1 Introduction

As the dynamical behaviour of a system is determined by the PES, characterization of the topography and topology of the PES is a prerequisite for understanding the dynamics. For example, to apply the master equation approach that we used for our model PES's in the previous chapter, one would need a complete sample of minima and transition states on the PES. Such sampling is only possible for very small clusters (up to $N \approx 13$) because of the exponential increase in the number of minima with size[64,65,162]. For larger clusters one would need some way to statistically characterize the PES in order to compensate for the incompleteness of any sample of stationary points. This would be akin to the method we used in §3.4 to reproduce the thermodynamics from an incomplete sample of minima.

Here we use the eigenvector-following method to obtain a comprehensive characterization of the M_{13} PES and its dependence on the range parameter, ρ_0 (§6.3), and to provide some typical downhill pathways for LJ clusters (§6.4). These surveys of the PES allow qualitative predictions of the effects of the range on the dynamics, and insight into the known relaxation behaviour of LJ clusters. Quantitative predictions await the application of the master equation method.

6.2 Traversing the Potential Energy Surface

The eigenvector-following technique[88] can find transition states on a PES by maximizing the energy along a chosen eigenvector of the Hessian whilst simultaneously minimizing the energy along all other eigenvectors. Once a transition state is located, the minima it connects can be found by taking small initial steps away from the stationary point along the eigenvector of the Hessian corresponding to the unique negative eigenvalue (in both the positive and negative directions) and then performing minimizations.

The technique we use to comprehensively search the PES is simple. From a starting minimum we search for transition states along the n_{ev} eigenvectors with the lowest eigenvalues in both positive and negative directions, and add the new minima that are connected by these transition states to our set of minima. We then repeat this process for all minima until until no new minima are found. The larger the value of n_{ev} (maximum $3N-6$), the more comprehensive the search will be. However, even using the maximum value of n_{ev} there is no guarantee that this approach will find all the minima on the PES. The method has been previously used to generate large samples of minima and transition states for small LJ clusters[162].

The second method we use involves a Monte Carlo walk between connected minima. First, from a starting minimum we randomly choose an eigenvector along which to search for a transition state; this choice is weighted towards those with lower eigenvalues, because a search along an eigenvector with a low eigenvalue generally converges to a transition state more rapidly. Once a transition state is found, we identify the minima it connects. Eigenvector-following occasionally finds a transition state unconnected to the original minimum, and so we check that the original minimum is at one end of the rearrangement pathway.

Having found a connected minimum, a decision whether to accept the step must then be taken. Here, we choose a Metropolis step criterion, which accepts moves with a probability of $\min[1, \exp(-\Delta E/kT)]$, where ΔE is the change in energy associated with the step[284]. There are many other possible step criteria that could be used. For example, the probability of acceptance could be related to the transition rate as calculated using RRKM theory, and so could be used to simulate the dynamics of the real cluster (assuming the density of states of the minimum and transition state could be calculated accurately). Once the decision to accept the step has been made the whole process is repeated, and a new transition state search is started. A record is kept of each transition state search, so that if the same step is attempted the search does not need to be repeated.

Techniques that search the PES by taking steps in configuration or phase space are hindered at low temperatures by the time scale separation between interwell and intrawell motion; this leads to trapping in local minima. Our method avoids this problem by removing the vibrational motion altogether.

To analyse the behaviour of our method further, the concept of a basin introduced by Kunz and Berry is useful[253,254]. These authors defined a basin as a set of connected minima that belong to sequences of minima which are monotonically decreasing in energy and which lead down to the lowest energy minimum in the basin. (This definition overlaps somewhat with the concept of a funnel that is used in the protein folding literature and which we discussed in Chapter 4.) The global minimum is at the bottom of the primary basin. Basins have a similar role in this 'minima space' to that played by minima in configuration space. However, there are far fewer basins than minima on the PES. The time scale for interbasin flow is likely to be slower than for intrabasin flow between minima[253,254]. Therefore, sufficiently deep secondary basins (basins that do not end at the global minimum) can act as traps (§5.4.4).

If a Monte Carlo walk in the minima space is performed at zero temperature, the system is 'quenched' to the bottom of a basin. If the number of basins on the PES is not too large, we might expect that a quench from a random configuration might lead to the global minimum, especially as it is likely that the primary basin would have the largest catchment area. This suggests that these quenches may be a useful global optimization tool. If a low rather than a zero temperature is used, the method would be able to escape from shallow basins, whilst not significantly compromising the favourability of downhill moves.

6.3 The PES of the 13-atom Morse Cluster

As we have noted in our consideration of Morse clusters in earlier chapters, decreasing the range of the potential increases the ruggedness of the PES. This effect is particularly noticeable in the number of stationary points on the PES (Table 2.1). Here we hope to quantify these ideas further by analysing the topologies of the M_{13} PES in detail. Given the ubiquity of rugged energy landscapes in a diverse range of fields—spin glasses, superconductors, protein folding and optimization problems such as the infamous travelling salesman problem—the results may be of wide interest[285].

The samples of M_{13} stationary points were produced by the method described in the previous section. For ρ_0=3, 4, 6, 10 and 14 we used as our values of n_{ev} 15, 15, 6, 3 and 2, respectively. The decreasing number of eigenvectors searched at shorter range was necessary because of the escalating requirements for computer time and disk space to generate and store the data for such large samples of stationary points. Consequently, the incompleteness of the samples is likely to increase with

TABLE 6.1: Some average properties of the M_{13} stationary point samples at ρ_0=3, 4, 6, 10 and 14. $\overline{\nu}$ is the geometric mean frequency, n_{ts} is the number of geometrically distinct transition states connected to a minimum, n_{gm} is the number of steps in minima space along the shortest path to the global minimum, S_{gm} is the total length in configuration space of the shortest pathway to the global minimum, ω is the magnitude of the imaginary frequency of a transition state, S is the length of a single rearrangement pathway, D is the displacement in configuration space between two connected minima, γ is the moment ratio of displacement, b_d is the smaller (downhill) barrier height, b_u is the larger (uphill) barrier height, ΔE is the difference in energy between two connected minima ($b_u = b_d + \Delta E$), and n_{basin} is the number of basins on the PES. $\overline{\nu}$, n_{ts}, n_{gm} and S_{gm} are averages over all minima; ω, S, D and γ, are averages over all transition states; and b_d, b_u and ΔE are averages over all non-degenerate transition states.

	$\rho_0 = 3$	$\rho_0 = 4$	$\rho_0 = 6$	$\rho_0 = 10$	$\rho_0 = 14$
$h\overline{\nu}/\epsilon$	0.216	0.340	0.682	1.843	3.680
n_{ts}	4.89	8.26	11.54	8.04	8.52
n_{gm}	1.00	1.38	2.40	3.65	3.70
S_{gm}/r_0	2.597	3.079	3.884	3.952	3.770
$h\omega/\epsilon$	0.184	0.262	0.469	1.051	1.450
S/r_0	3.012	2.905	1.874	1.119	1.083
D/r_0	1.607	1.477	1.169	0.842	0.819
b_d/ϵ	0.114	0.483	0.545	0.585	0.786
b_u/ϵ	4.512	3.693	2.087	1.473	1.540
$\Delta E/\epsilon$	4.398	3.210	1.542	0.888	0.786
$13/\gamma$	7.161	5.269	4.748	5.051	4.889
n_{basin}	1	1	3	54	262

ρ_0 and be greater for the transition states than minima. The size of the samples is given in Table 2.1 and some of the average properties are catalogued in Table 6.1. Some properties have a fairly simple dependence on ρ_0. For example, the increase in the mean vibrational frequency as the range decreases correlates with the increased curvature of the pair potential at its minimum (Figure 2.2).

More interesting are those properties that give insight into the global topography of the PES. As can be seen from Figure 4.4 the energy gap between the global minimum, the 13-atom icosahedron, and the other low-lying minima decreases as ρ_0 is increased. This flattening of the surface is also apparent in the average values of ΔE, the difference in energy between two connected minima; ΔE is effectively

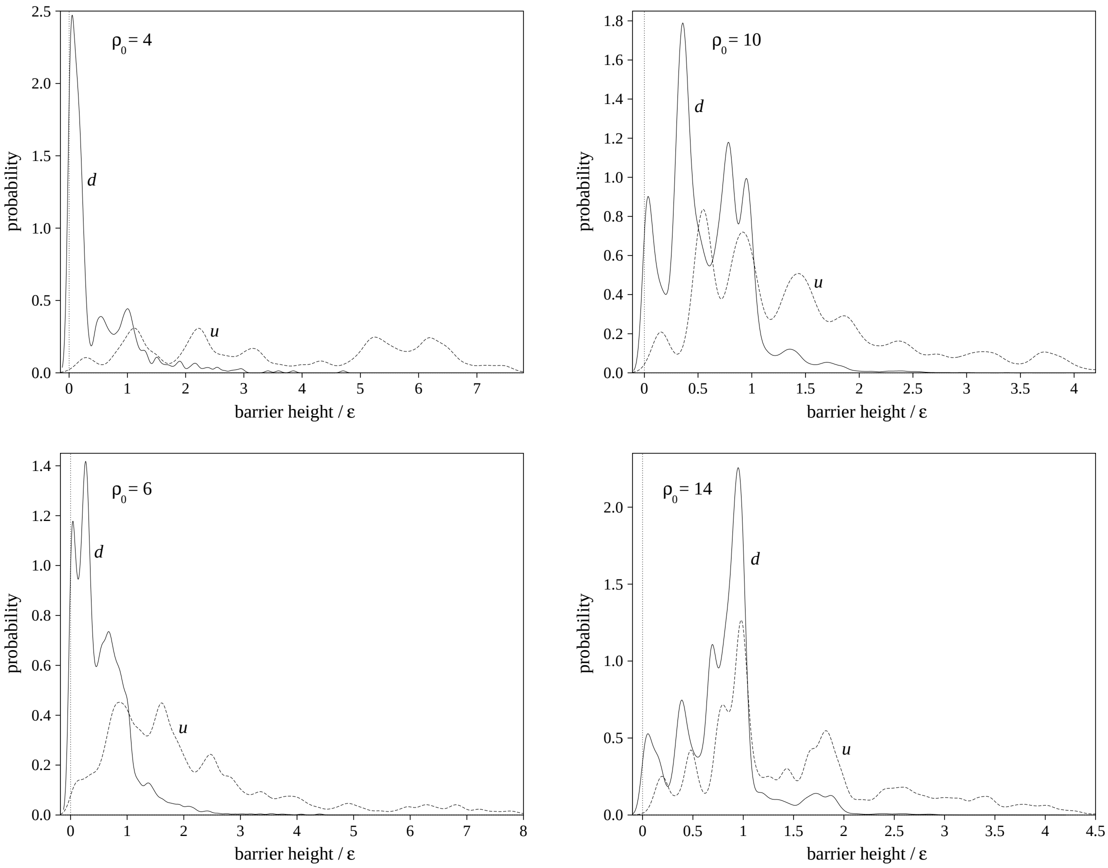

FIGURE 6.1: Probability distributions of the barrier heights of uphill (dashed line) and downhill (solid line) rearrangements for M_{13} at ρ_0=4, 6, 10 and 14, as marked. Transition states mediating degenerate rearrangements have been excluded from the samples.

a local measure of the slope of the PES.* The averages of the barrier heights show that the barrier to go downhill (b_d) increases with ρ_0. At ρ_0=4, the probability distribution of b_d is dominated by the low barrier peak (Figure 6.1), but as ρ_0 increases the magnitude of this peak diminishes. The greater similarity between the distributions for b_d and b_u at larger ρ_0 is a reflection of the smaller value of ΔE. We expect, based on the results of Chapter 5, that the combined effect of the larger downhill barriers and the flatter PES will be to make relaxation to the global minimum more difficult at shorter range.

In a comparison of the topographies of Lennard-Jones and potassium chloride clusters, it was noted that the rearrangements for potassium chloride clusters were

*For the distributions and averages of b_d, b_u and ΔE the degenerate rearrangements (that join permutational isomers of the same minimum) are excluded from the sample because they contain no information about structural relaxation, and simply obscure the changes to the topology of the PES. The fraction of transition states that mediate degenerate rearrangements varies from 38% for ρ_0=3 to 1% for ρ_0=14.

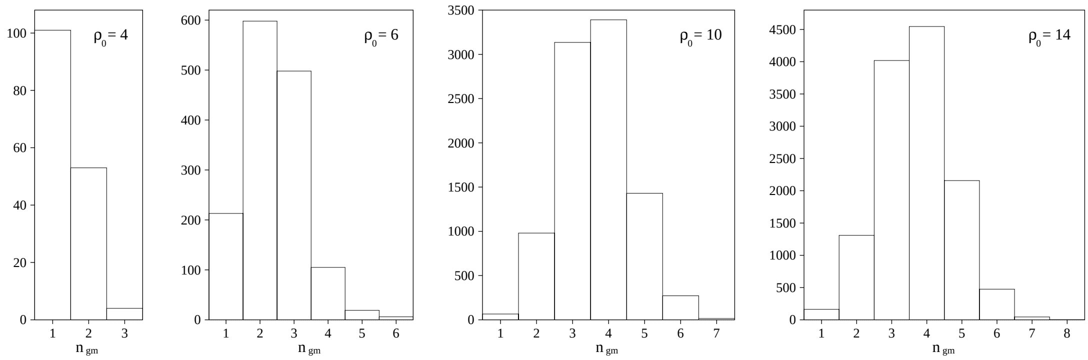

FIGURE 6.2: Histograms of n_{gm}, the number of steps a minimum is away from the global minimum, for M_{13} at ρ_0=4, 6, 10 and 14, as marked.

much more cooperative[252]. It was suggested that this might have been one of the reasons for the greater ease with which the potassium chloride clusters could reach the global minimum. The moment ratio of displacement, γ, can be used to measure the cooperativity of a rearrangement. It is defined by[286]

$$\gamma = \frac{N\sum_i \left[Q_i(s) - Q_i(t)\right]^4}{\left(\sum_i \left[Q_i(s) - Q_i(t)\right]^2\right)^2}, \tag{6.1}$$

where $Q_i(s)$ is the value of the nuclear Cartesian coordinate Q_i for minimum s, etc. γ was evaluated using the relative positions of the two minima at the end-points. If only a single atom moves then $\gamma = N$ and the rearrangement is strongly localized, while if all atoms move through the same distance then $\gamma = 1$ and the process is completely cooperative. N/γ therefore can be interpreted as the number of atoms involved in the rearrangement. Somewhat surprisingly, apart from the greater cooperativity at ρ_0=3, γ does not depend significantly on the range of the potential (Table 6.1). This is in contrast to a study which compared rearrangements of LJ_{55} and $(C_{60})_{55}$ clusters, which found that cooperative rearrangements were much less likely for $(C_{60})_{55}$ clusters[90]. This difference may reflect the fact that the structure of small clusters is less dependent on the range than for larger clusters.

The shortest reaction pathway to the global minimum was calculated for each minimum on the PES. If we look at n_{gm}, the number of steps between minima along one of these pathways, it is clear that n_{gm} increases as the range decreases (Figure 6.2). At ρ_0=3 all the minima are directly connected to the global minimum, yet at ρ_0=14, a minimum can be as far as eight steps away. The n_{gm} histograms also show that the connectivity patterns for the M_{13} PES are quite different from the standard model PES that we considered in Chapter 5 for which the number of minima increased exponentially with the number of steps away from

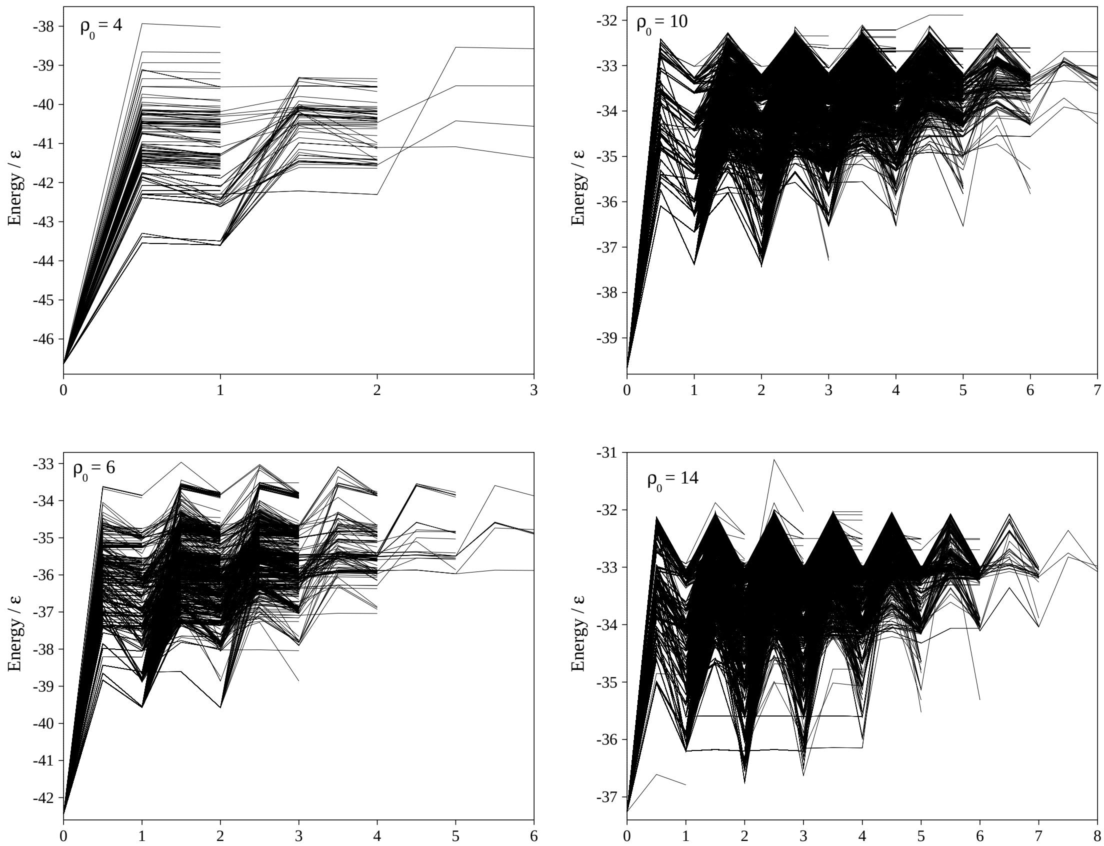

FIGURE 6.3: Shortest pathways to the global minimum for each minimum of M_{13} at ρ_0=4, 6, 10 and 14 as marked. The reaction coordinate is the number of steps away from the global minimum. Half integer values correspond to transition states.

the global minimum. It is also interesting to note the large number of minima that are directly connected to the global minimum. For example, at ρ_0=6 we found 568 geometrically distinct transition states which connect the icosahedron to 213 geometrically distinct minima. If one takes into account the reaction path degeneracy, the number of transition states surrounding a single permutational isomer of the icosahedron is at least 67 836.

In Figure 6.3, we show the shortest reaction path to the global minimum for each minimum. Again the larger barrier heights and the increased flatness of the PES are apparent at short range. At ρ_0=14 there are clearly some pathways for which the minima do not monotonically decrease in energy as the global minimum is approached. This will be considered further when we examine the basin structure of the PES.

Although n_{gm} increases with ρ_0 the average total length of the reaction paths in configuration space (S_{gm}) is relatively constant for $\rho_0 \geq 6$, and for smaller ρ_0

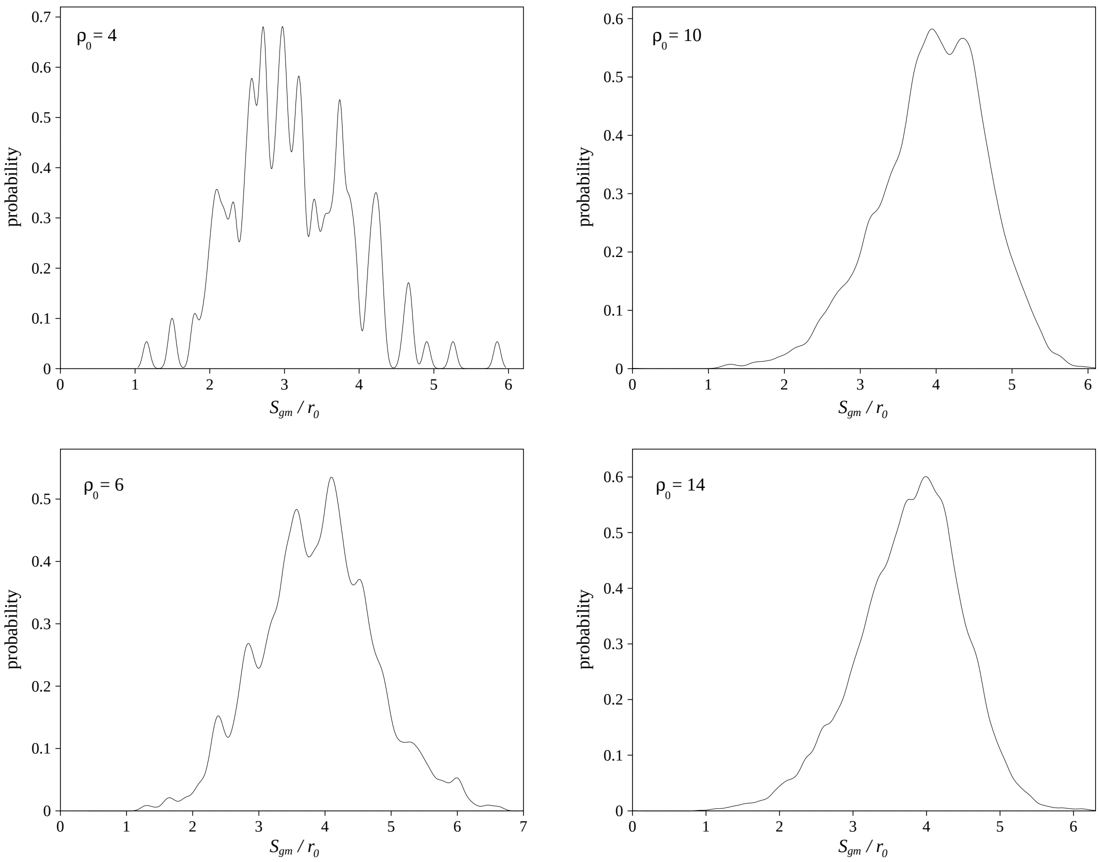

FIGURE 6.4: Probability distributions of S_{gm}, the length of the shortest pathway from a minimum to the global minimum, for M_{13} at ρ_0=4, 6, 10 and 14 as marked.

shows a much weaker dependence on the range than n_{gm} (Table 6.1 and Figure 6.4). This is not too surprising if we consider the dependence of the path length for a single rearrangement on ρ_0: this length decreases significantly as the range is reduced (Figure 6.5). The pathways simply become more rugged rather than longer: more transition states must be crossed.

The topology of the surface was further analysed in terms of the structure of the basins on the PES. For ρ_0=3 and 4, every minimum lies on a sequence of minima which are monotonically decreasing in energy and lead down to the global minimum; the PES consists of a single basin. For ρ_0=6 all but two of the minima lie on such monotonic sequences. By Kunz and Berry's definition these two minima also represent basin bottoms, albeit very shallow; only one step needs to be taken to reach a minimum in the basin surrounding the icosahedron. For ρ_0=10 and 14 many more shallow basins appear on the PES (Table 6.1). Despite this increase in the number of basins, 96.8% of the minima located are in the icosahedral basin for ρ_0=14 (Figure 6.6e).

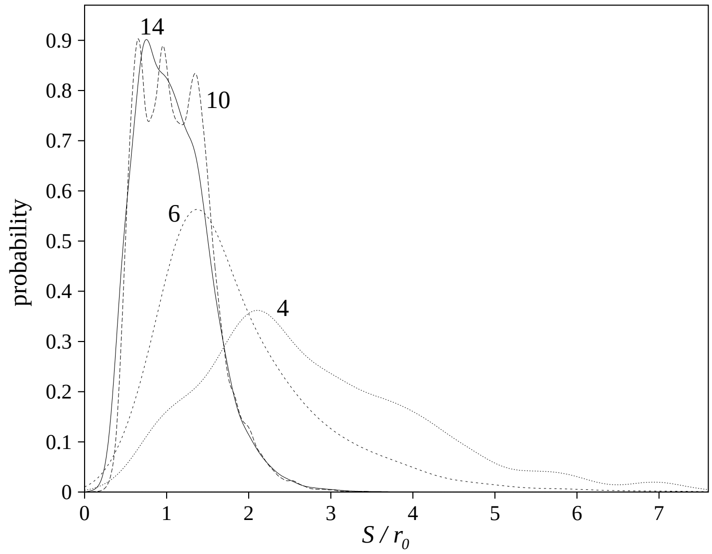

FIGURE 6.5: Probability distributions of S, the length of a single rearrangement pathway, for the transition states of M_{13} at ρ_0=4, 6, 10 and 14 as marked.

One consequence of the definition of a basin is that it is possible for a minimum to lie on monotonic sequences which lead down to the bottom of different basins. Indeed high energy minima may lie in numerous basins (Figure 6.6f). In this regard the division of minima space into basins differs from the division of configuration space into wells surrounding minima, since there is no equivalent of the steepest descent path which uniquely maps each point in configuration space to a minimum. Instead the division of minima space is more like a Venn diagram where overlap can occur between regions.

One method to analyse this basin structure is with 'tree' diagrams (Figure 6.6); these are in some ways similar to the equilibration trees considered in Chapter 5. Two basins are considered to become 'connected' and to form a new metabasin when the energy is that of the lowest energy minimum which lies in both basins. Each point in the tree diagram represents a basin or the creation of a new metabasin, and the nodes occurs at the energies at which the basins or metabasins become connected. The tree diagrams, therefore, follow the pattern of connections that occurs between basins and metabasins as the energy is increased.

It is noticeable that in the tree diagrams virtually all the basins are directly connected to the line corresponding to the metabasin of the global minimum, i.e. the basin which requires least energy to enter is the metabasin of the global minimum. The basin surrounding the global minimum is clearly the dominant feature even on the more rugged PES's for ρ_0=10 and 14. Furthermore, many of

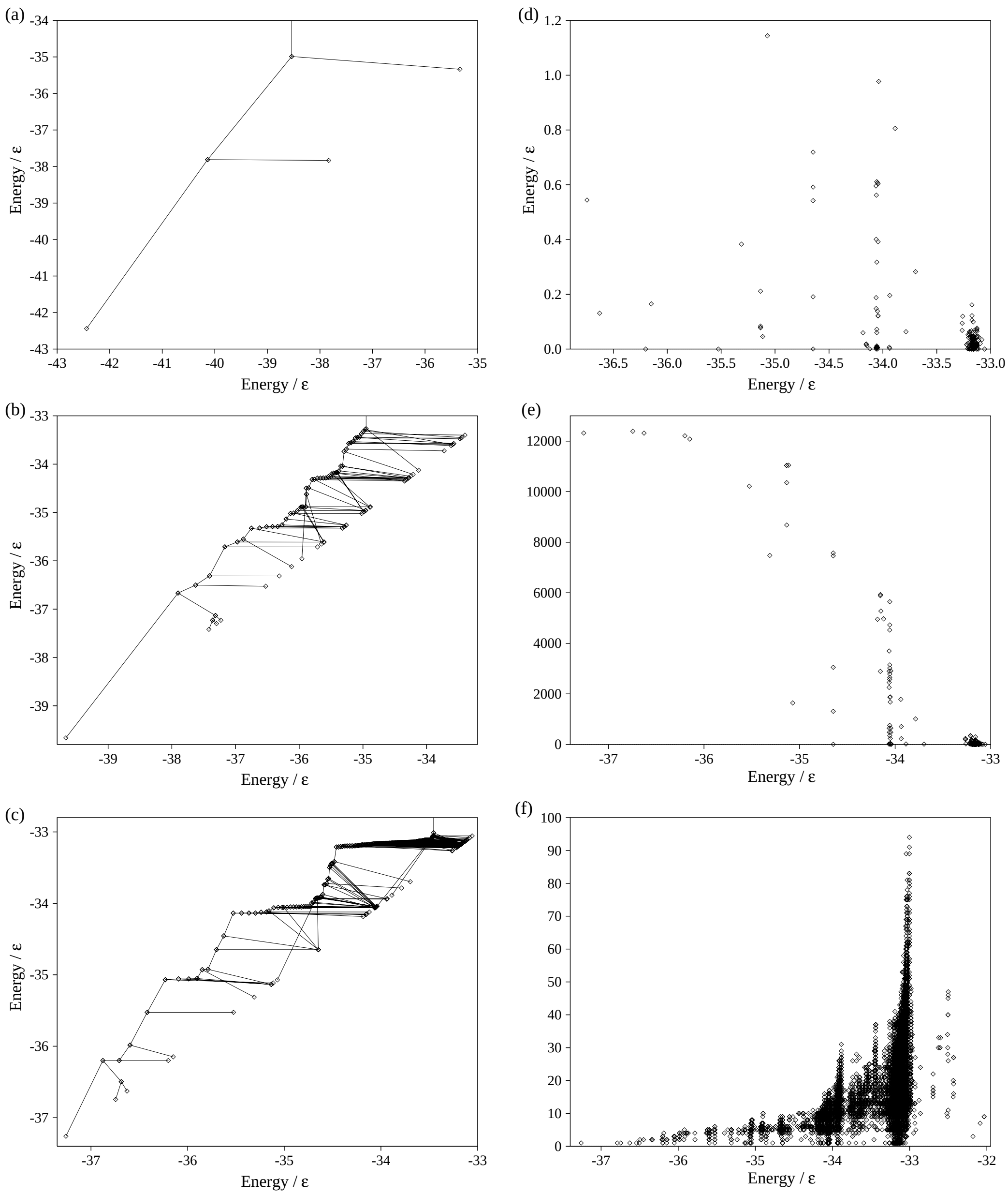

Figure 6.6: 'Tree' diagrams showing the basin structure for M_{13} at (a) ρ_0=6, (b) ρ_0=10, and (c) ρ_0=14. The endpoints are at the energies of the minima at the bottoms of the basin. Nodes occur when two basins or metabasins become connected; The y coordinate of the node corresponds to the energy of the lowest energy minimum which lies in both (meta)basins, and the x coordinate to the average energy of the all the basin bottoms in the resulting metabasin. Scatter plots of (d) the energy (relative to the bottom of a basin) of the lowest energy minimum which is in both the basin concerned and a lower energy basin against the basin energy, (e) the number of minima in a basin against the basin energy and (f) the number of basins a minimum belongs to against the energy of the minimum for M_{13} at ρ_0=14

the lines joining a basin to the icosahedral basin are virtually horizontal implying that the depth of most basins (measured in terms of the energy, relative to the basin bottom, of the lowest energy minimum that is also in another basin) is small (Figure 6.6d). The average depths for ρ_0=10 and 14 are 0.237 and 0.067 ϵ, respectively. Most of the basins are not sufficiently deep to act as effective traps. The lower average depth for ρ_0=14 results from the large number of very shallow basins at high energy; 163 of the 262 basins lie above $-33.5\,\epsilon$.

Although the PES's at ρ_0=10 and 14 involve a large number of basins, these PES's do not equate with the multiple funnel scenarios outlined in §5.4 since the basins are too shallow for them to be categorized as separate funnels. However, their roughness is still likely to hinder relaxation to the global minimum, even if not to as large an extent as multiple funnels.

6.4 Pathways for Lennard-Jones Clusters

Our second method for surveying the PES has been applied to LJ_{13}, LJ_{38} and LJ_{55}. For the 13- and 55-atom clusters the global minima are Mackay icosahedra. We also chose to study LJ_{38} because, unusually for small clusters, it does not have an icosahedral global minimum but instead an fcc truncated octahedron (structure 38D of Chapter 2) is lowest in energy[70,71]. This cluster therefore represents a relatively difficult test for a global optimization method.

The energy profiles for typical low temperature quenches in minima space performed from random starting configurations are shown in Figure 6.7 for the three clusters. The quenches for the 13-atom cluster typically find the icosahedral global minimum in three or four accepted steps. This is not surprising given the relative simplicity of the PES; the number of minima on the surface[162] is probably of the order of 1500 and none of the minima are more than four steps away from the global minimum.[†]

The quenches for LJ_{55} also find the global minimum, although the pathway and the number of steps is inevitably larger because of the increased system size. Still it is a remarkable feature of this PES that the global minimum is so easy to find considering there are probably of the order of 10^{21} minima on the PES. In the last part of the pathway shown in Figure 6.7c the cluster finds the Mackay icosahedron in two steps from a low energy liquid-like minimum, rather than by

[†]This result is based upon an analysis of the LJ_{13} PES similar to that performed for M_{13} in §6.3. Using n_{ev}=15, 1467 minima and 12 435 transition states were found.

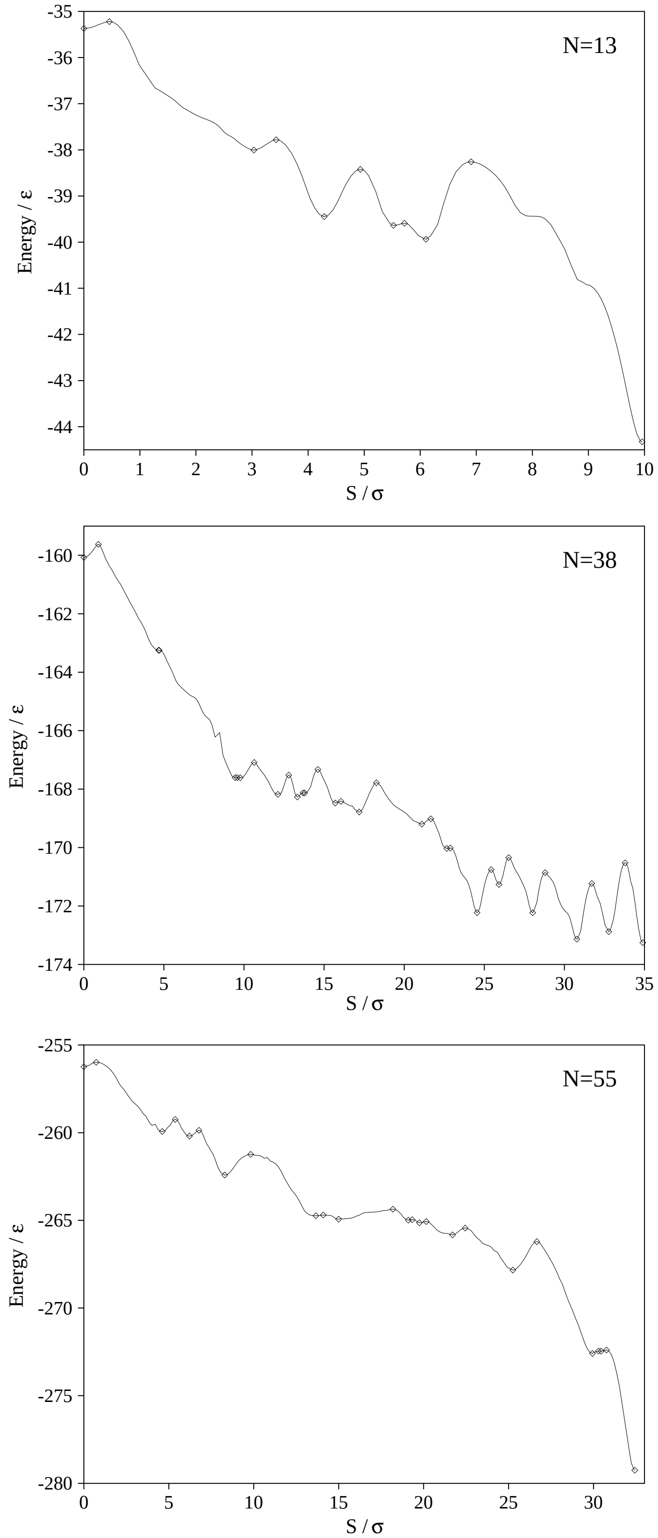

Figure 6.7: Reaction profiles of typical downhill pathways from a random minimum to the lowest energy icosahedral minimum for LJ_{13}, LJ_{38} and LJ_{55}. Stationary points are denoted by diamonds. S is the integrated path length along the reaction pathway[90]

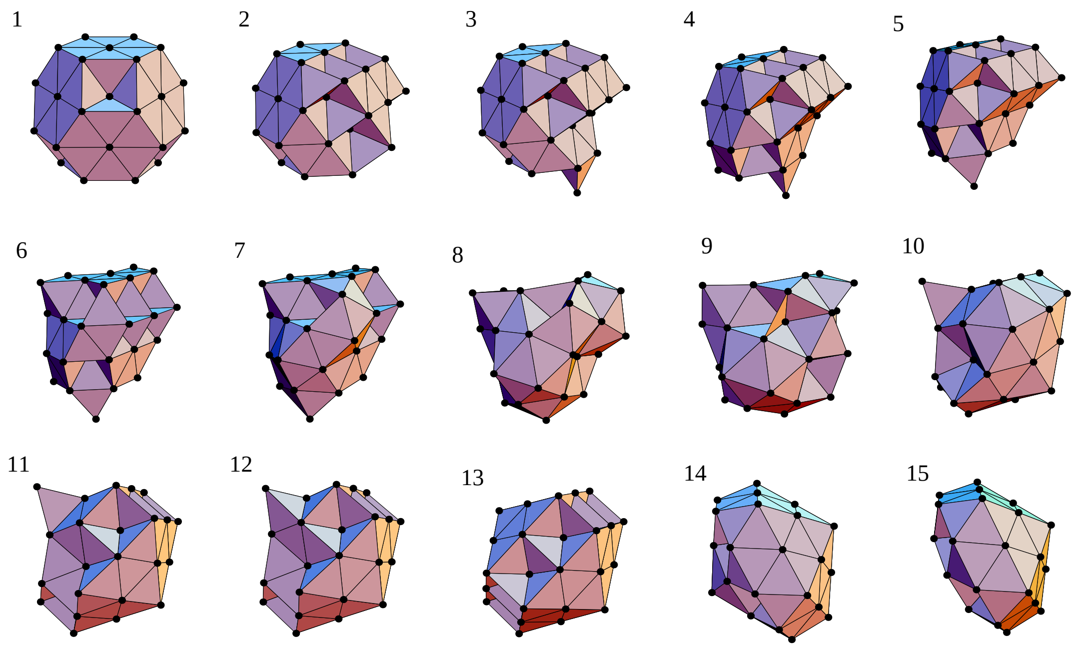

Figure 6.8: Minima on the LJ_{38} pathway from the truncated octahedron to the lowest energy icosahedral minimum. The minima are numbered by their position along the pathway

passing through defective Mackay icosahedra as was observed for some of the other pathways.

For LJ_{38} the system never finds the fcc global minimum but instead the quenches always lead into the basin of icosahedral minima and down to the lowest energy icosahedral minimum (structure 38E of Chapter 2). Although this represents a failure of the method as a global optimization tool, it provides us with some interesting information about the topography of the PES. It seems that the basin containing the icosahedral minima is much more easily accessed from higher energy minima than the basin leading down to the fcc minima. This is probably a result of the greater structural similarity between the icosahedral structures and the liquid that we discussed in §4.4.

One difference between the quench pathway for LJ_{38} and that of the other two clusters is that in the last stages of the pathway the system has to search through the low energy icosahedral isomers. The bottom of the icosahedral basin is flatter than for LJ_{13} and LJ_{55}, both of which have global minima that are significantly lower in energy than the next lowest energy minimum, making the last stages of global optimization easier. For comparison, the energy gaps between the lowest energy icosahedral minima are $2.644\,\epsilon$, $0.118\,\epsilon$ and $2.855\,\epsilon$ for LJ_{13}, LJ_{38} and LJ_{55},

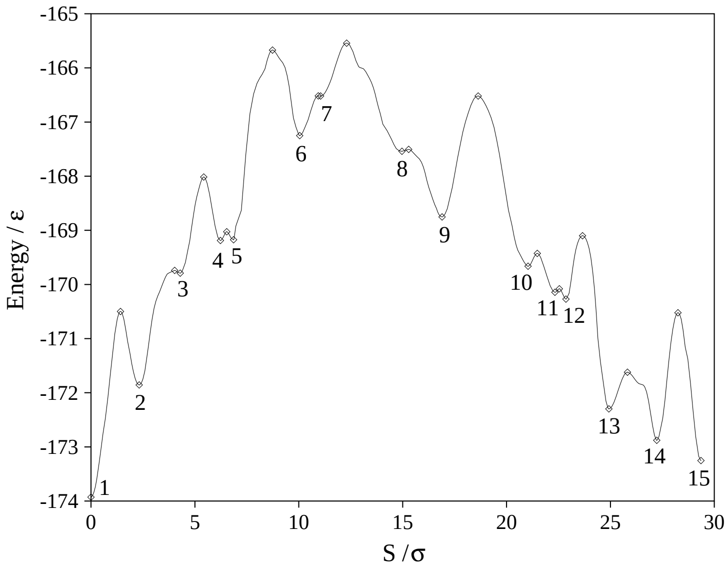

FIGURE 6.9: Reaction profile of a pathway on the LJ_{38} PES from the truncated octahedron to the lowest energy icosahedral minimum. Stationary points are denoted by diamonds. The minima are numbered by their position along the pathway

respectively.

As for M_{75} at ρ_0=6 (§2.4), it may be that the 38-atom truncated octahedron is the free energy global minimum only at low temperature. If this is the case, we would expect a high temperature Monte Carlo walk in minima space starting from the truncated octahedron to escape from the fcc basin and pass into the icosahedral basin, and this is indeed what we observed. The length of the initial pathway between the two lowest energy structures produced by this method was about $100\,\sigma$. However, by performing quenches on either side of the barrier, the pathway was significantly shortened. The resulting pathway is illustrated in Figures 6.8 and 6.9. The LJ_{38} PES clearly has similarities to some of the multiple funnels scenarios considered in §5.4.4. From the cross-section (Figure 6.9) it does appear that the basin surrounding the truncated octahedron is narrower than the icosahedral basin, which is what would be expected given the propensity for LJ_{38} to go into the icosahedral basin on relaxation.

In the structural transformation the truncated octahedron initially undergoes a series of rearrangements that take it to the high energy hexagonal close-packed minimum 6. This structure then collapses to a polytetrahedral structure typical of the liquid-like state, which becomes more and more ordered until it reaches the decahedral structure 11. After two localized rearrangements, the decahedral minimum 13 is then converted to an icosahedral minimum by a multiple squarediamond process in which one half of the structure is rotated by $\pi/5$ about the decahedral axis.

In electron microscopy studies of metal clusters supported on a surface, transformations are often observed between icosahedral, decahedral and fcc structures[1]. The pathway we have found here, although for a cluster much smaller than those observed experimentally, is probably fairly typical of the complex series of rearrangements and high energy barriers that need to be overcome to move between ordered structures with different morphologies.